# Magnetic moments of $^{68}$Cu$^{g,m}$ and $^{70}$Cu$^{g,m_1,m_2}$ nuclei measured by in-source laser spectroscopy

L. Weissman,* U. Köster, R. Catherall, S. Franchoo, U. Georg, and O. Jonsson
*ISOLDE, CERN, 1211 Genève 23, Switzerland*

V. N. Fedoseyev and V. I. Mishin
*Institute of Spectroscopy, Russian Academy of Sciences, 142190 Troitsk, Russia*

M. D. Seliverstov
*Petersburg Nuclear Physics Institute, 188350, Gatchina, St. Petersburg, Russia*

J. Van Roosbroeck, S. Gheysen, M. Huyse, K. Kruglov, G. Neyens, and P. Van Duppen
*Instituut voor Kern-en Stralingsfysica, University of Leuven, B-3001 Leuven, Belgium*

IS365 Collaboration and ISOLDE Collaboration

We have obtained information on the atomic hyperfine splitting and, hence, on magnetic moments in neutron-rich $^{68,70}$Cu isotopes by scanning the frequency of the narrow-band laser of the first excitation step in the resonance ionization laser ion source. The deduced magnetic moments are $\mu(^{68}\text{Cu}^g, I^\pi = 1^+) = +2.48(2) \times (7)\mu_N$, $\mu(^{68}\text{Cu}^m, I^\pi = 6^-) = +1.24(4)(6)\mu_N$, and $\mu(^{70}\text{Cu}^{m_2}, I^\pi = 1^+) = +1.86(4)(6)\mu_N$, $\mu[^{70}\text{Cu}^g, I^\pi = (6^-)] = (+)1.50(7)(8)\mu_N$. The results of the scans analysis points out the existence of a new isomer, $^{70}$Cu$^{m_1}$. Its deduced magnetic moment is $(-)3.50(7)(11)\mu_N$, in good agreement with the $I^\pi = 3^-$ assignment. The method of in-source atomic spectroscopy, as well as the analysis of the obtained data, is described. The results are discussed in terms of single-particle configurations coupled to the $^{68}$Ni core.

## I. INTRODUCTION

A subshell closure at $N=40$ has been the subject of intensive studies in recent years. This interest was triggered by the observation of a high excitation energy of the first $2^+$ level in $^{68}$Ni [1]. To investigate the strength of the subshell closure many recent studies involved in-beam experiments [2–4] and $\beta$-decay spectroscopy [5–8] of nuclei in the region around $Z=28$, $N=40$. The results of these experiments suggest that the stabilizing effect of the $N=40$ shell gap disappears with the addition of a single nucleon [7]. In this context, measurements of magnetic moments of nuclei in the vicinity of $^{68}$Ni are of special interest, since they essentially probe the single-particle degrees of freedom and provide new information, complementary to that obtained from nuclear spectroscopy.

Magnetic moments of $^{67}$Ni ($T_{1/2}=21$ s) and $^{69}$Cu ($T_{1/2}=3$ min) were measured recently in an on-line $\beta$-NMR experiment on oriented nuclei (NMR-ON) [9] and $g$ factors of isomeric states in these nuclei were measured via the time-differential perturbed angular distribution (TDPAD) on isomeric projectile fragments [10,11]. The applicability of these techniques has some limitations: NMR-ON is limited to longer-lived activities, and TDPAD is only applicable to short-lived microsecond isomers. Atomic spectroscopy in a resonance ionization laser ion source (RILIS) presents an alternative technique, allowing a rough determination of $g$

factors of any nuclei produced by the ISOL method. Most of the recent results from $\beta$-decay spectroscopy measurements in the region of neutron-rich Ni, Cu, and Co [5–8,12] were obtained at the LISOL and ISOLDE facilities by using resonance ionization laser ion sources [13,14]. The high chemical selectivity of two- or three-steps resonance ionization processes as well as a high ionization efficiency makes the RILIS a very powerful tool for the production of exotic nuclear beams. Moreover, laser ionization in a RILIS can be used for in-source atomic spectroscopy of rare short-lived isotopes.

The idea of atomic in-source spectroscopy in a RILIS can be described as follows. Two or three lasers at resonant frequencies ionize the atoms of interest. A narrow-bandwidth laser is used for the first excitation step allowing to probe the hyperfine splittings (HFS) of the atomic states by scanning the frequency of the first excitation step and by simultaneously monitoring the yield of the produced ions.

This method was pioneered at the Leningrad Nuclear Physics Institute [15]. In those studies the isotopic shifts (in some cases the HFS) were measured for the $^{153,154}$Tm and $^{153-156}$Yb isotopes [15–17]. In the first application of in-source atomic spectroscopy at the ISOLDE RILIS, the HFS of several silver isomers and the isotope shifts of $^{7-14}$Be isotopes were measured [18]. In-source atomic spectroscopy of neutron-rich copper isotopes, as well as the possibility of isomer separation, was recently demonstrated at the ISOLDE RILIS [19].

In general, due to the high Doppler broadening in the hot cavity of the RILIS the accuracy of these measurements can-

---

*Corresponding author. Email address: leonid.weissman@cern.ch
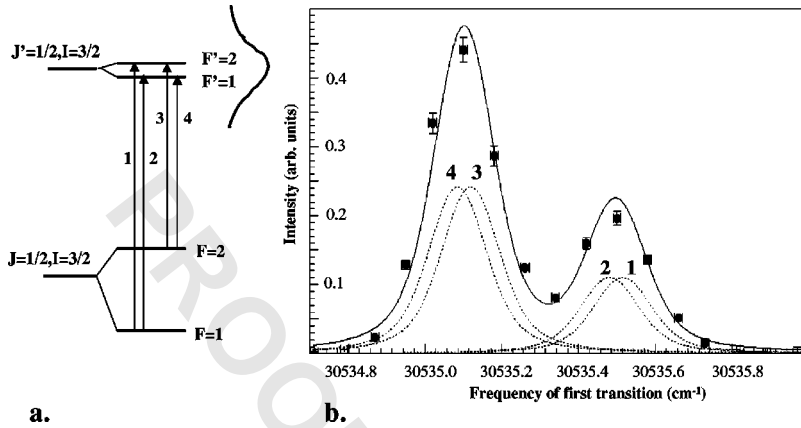
**65** 0143XX-1

FIG. 1. (a) A schematic illustration of the four atomic transitions covered by the scanned frequency range. The linewidth of the first laser allows to resolve the ground-state $HFS_g$, but not the excited state $HFS_{ex}$. (b) A typical scanning curve for the stable $^{65}$Cu isotope with 1.5 mW power of the first ionizing step. Here and in all the following figures the measured counting rate as a function of the scanning frequency is given in arbitrary units. The experimental errors are mainly due to fluctuations in the laser power.

not compete with the precision $\beta$-NMR measurements or with collinear laser spectroscopy [20]. However, an advantage of the in-source method is its high efficiency and, hence, the opportunity to access weakly produced short-lived exotic nuclei. In this work we concentrate on the analysis of in-source spectroscopy data and discussion of the magnetic moments obtained for the $^{68,70}$Cu nuclei in the neighborhood of the $^{68}$Ni nucleus. The results of similar measurements in more exotic neutron-rich copper isotopes will be addressed elsewhere [21].

## II. EXPERIMENT, DATA ANALYSIS, AND RESULTS

### A. Experimental details

In the following we present a brief description of the experimental setup; the details of the setup are given in Ref. [19]. Neutron-rich copper isotopes were produced in fission reactions induced by a pulsed beam of 1 GeV protons (average current $2\,\mu A$) impinging on an ISOLDE uranium carbide target (50 g/cm$^2$U). The reaction products diffuse from the target heated to about 2000 °C and are guided to an ion source. Two laser beams at 327.4 nm and 287.9 nm wavelength interacted with the copper atoms exciting them from the $3d^{10}4s$ $^2S_{1/2}$ ground state via the intermediate $3d^{10}4p$ $^2P_{1/2}$ state to the $3d^94s5s$ $^2D_{3/2}$ autoionizing state leading to ionization. The dye lasers were pumped by copper-vapor lasers. For the first-step transition a narrowband laser with a bandwidth of 1.2 GHz was used. Its frequency was scanned up to about 20 GHz to probe the HF's of the ground and the first excited atomic states. For the second step a broadband 24 GHz dye laser was used. The frequency of the lasers was monitored with an ATOS LM-007 lambda meter (resolution $\leqslant 300$ MHz). The duration of the laser pulses and repetition rate were 15 ns and 11 kHz, respectively. The ionization efficiency for copper atoms was found in off-line tests to be more than 7% [22]. After leaving the ion source cavity the ions are accelerated by a 60 kV voltage and mass-separated. The mass-separated ions were implanted into a tape and swiftly transported to a detector setup. The yield of radioactive isotopes, as a function of the first-step frequency, was derived from the intensities of $\beta$-delayed $\gamma$ transitions. A 30% efficiency Ge(Li) detector and a $4\pi$ cylindrical $\beta$ detector surrounding the tape were used for this purpose. Several measurements were performed

for each frequency setting to average over possible yield fluctuations. The measurement time was optimized for each isotope separately. The background in the Ge detector from the decay of surface ionized Ga isobars is negligible at these masses. The contribution of surface ionized copper ions was also negligible.

The main concern of these measurements was to ensure that possible drifts of the lasers' power would not affect the shape of the scanning curves. The ISOLDE general purpose mass-separator has a movable beam deflector system which allows simultaneous measurement of two or three isotopes at different beam lines. During the frequency scans the current of stable $^{63}$Cu or $^{65}$Cu isotopes was measured in a Faraday cup at the low-mass beam line while the yield of radioactive $^{68,70}$Cu isotopes was measured by a $\beta$-$\gamma$ detector setup at the central-mass beam line. This arrangement allows to reject measurements affected by a drift of the laser power and to monitor other possible systematic errors by comparing the scans obtained with stable isotopes.

### B. Analysis of the scanning curves for the stable isotopes

The first-step frequency scan covers four optical resonance transitions from the hyperfine levels of the ground state ($F=2$ and $F=1$) to the corresponding levels of the excited state ($F'=2$ and $F'=1$), see Fig. 1(a). The in-source measurements do not always allow to resolve all hyperfine structure components. This is due to the Doppler broadening of the linewidth in the hot cavity of the RILIS as well as due to power broadening caused by saturation of the resonant 327.4 nm transition. While the Doppler broadening is determined by the temperature of the hot cavity and the atomic mass ($\approx 3.8$ GHz at 2000 °C for $^{65-70}$Cu), the power broadening can be reduced significantly by decreasing the power of the first laser ionizing step and thus compromizing on the ion yield.

As a result of such a scan, the two atomic transitions that start from the two ground-state hyperfine levels are found to be resolved [lines 1–3 and 2–4 in Fig. 1(a)], but the two atomic transitions to a particular excited hyperfine level (e.g., lines 1–2 and 3–4) are not. The HFS of the ground and excited states in the stable isotopes are well known [23,24] and thus provide a test of the analysis procedure. A typical curve obtained for the stable isotope $^{65}$Cu, corresponding to
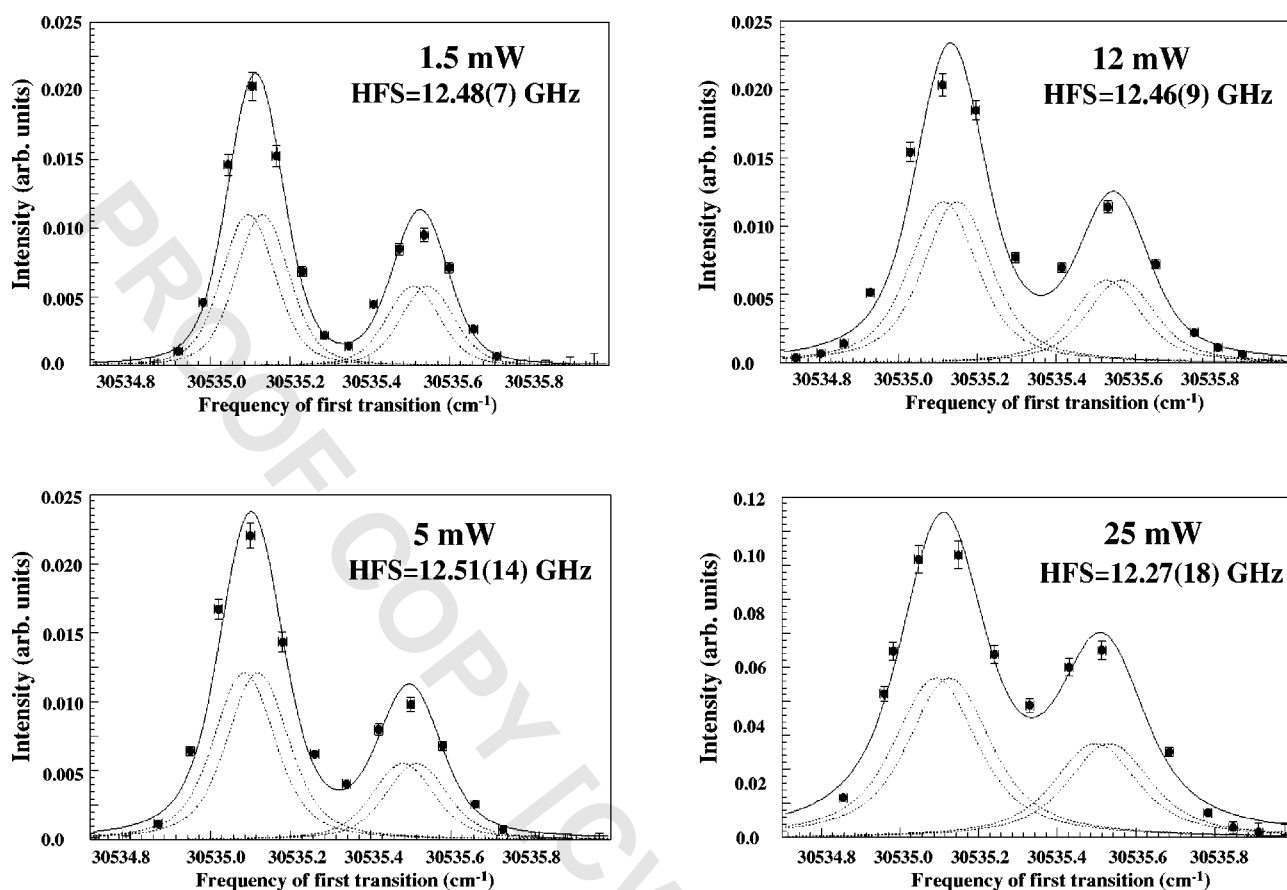
FIG. 2. The $^{65}$Cu scanning curves as a function of the laser power of the first resonant excitation step. The data are fitted assuming "equal intensities" of the nonresolved transitions. The deduced HFS$_g$ and fit errors are quoted.

a laser power of 1.5 mW, is shown in Fig. 1(b). The experimental errors are mostly due to yield variations caused by fluctuations of the laser power. The scanning curve was fitted by four Voigt curves corresponding to the line shape of the four resonance atomic transitions. Each of the Voigt curves is a convolution of a Gaussian with a fixed 3.8 GHz width (Doppler broadening) and Lorentzian width used as a free parameter (power broadening). The ratio of the first excited to the ground-state HFS in the copper atom does not depend on the isotope and is known to be HFS$_{ex}$/HFS$_g$ = 0.086 [23,24]. This ratio allows to put constraints on the relative positions of the four Voigtian peaks, leaving only

TABLE I. The parameters obtained from fitting the $^{65}$Cu HFS scans taken at various laser powers. An additional 3% scattering error is adopted in the final HFS value.

| Power (mW) | HFS$_g$ (GHz) | Central frequency (cm$^{-1}$) | Ratio of peak amplitudes |
|---|---|---|---|
| 1.5 | 12.48(7) | 30535.24(2) | 1.90±0.11 |
| 5 | 12.46(9) | 30535.27(2) | 1.91±0.11 |
| 12 | 12.51(14) | 30535.26(2) | 1.95±0.12 |
| 25 | 12.27(37) | 30535.25(2) | 1.70±0.13 |
| Tabulated value | 12.5697 | 30535.302 | |

[a]Reference [23].

two parameters to fit the four peak positions: the ground-state HFS$_g$ of the $^A$Cu atom and the position of one peak. Attempts to fit the scanning curve with the remaining eight free parameters (the position of the lowest frequency peak, the HFS$_g$, the width of the Lorentzian part of the Voigt curves, four independent amplitudes of the Voigt peaks, and a constant background) failed to produce the correct values of the known HFS$_g$($^{65}$Cu) = 12.5697 GHz [23]. Therefore we have tried a simple approach to further reduce the number of fit parameters. As the transitions to the excited hyperfine splitting levels are not resolved because the laser linewidth is much larger than the HFS$_{ex}$ (4 GHz compared to 1.2 GHz), we have assumed that the intensities of lines 1 and 2 (lines 3 and lines 4.) originated from the same hyperfine level are equal. This constraint leads to a simplified fitting procedure of the scanning curve, which we refer as an "equal intensity" fit, with six free parameters. The result of such a fit gives 12.48(7) GHz [Fig. 1(b)] for the HFS$_g$($^{65}$Cu), in a good agreement with the tabulated value.

To check the stability of the fit we performed several scans for the stable isotopes at various values of the laser power. As shown in Fig. 2 the shape of the scan curves changes significantly with increasing power. At the highest laser power the peak amplitude ratio approaches the expected saturation value which is the ratio of the statistical weights of the $F=2$ and $F=1$ hyperfine levels, 5/3. However, the val-

ues obtained for the HFS$_g$ and the central frequency stay constant within the errors, until the highest laser power is applied (see Table I). These results give confidence in the analysis procedure. The errors quoted on the pictures and in Table I are as deduced from a $\chi^2$ fit. In addition to the fit errors we also introduce a conservative scattering error of 3%, which reflects a possible systematic uncertainty due to changes of the HFS value with the laser power.

Apart from these simple, "equal intensity" fits we have also attempted to calculate relative intensity ratios for the four atomic transitions and to use these ratios in the fitting procedure. Brief details on these "relative intensity" fits are given in the appendix.

### C. Results for radioactive $^{68}$Cu$^{g,m}$ and $^{70}$Cu$^{g,m_1,m_2}$ isotopes

For a typical 50 mW laser power in the first resonant excitation step, the yields of $^{68}$Cu$^g$ and $^{68}$Cu$^m$ were 2.3 $\times 10^7$ and $1.1\times 10^8$ ions per $\mu$C of the proton beam. The corresponding yields of $^{70}$Cu$^g$, $^{70}$Cu$^{m_1}$ and $^{70}$Cu$^{m_2}$ isomers (see below) were $9.0\times 10^7, 3.8\times 10^6$, and $1.8\times 10^7$ atoms, respectively. The use of a Ge $\gamma$ detector allows the measurement of the HFS of both isomers during the same frequency scan by monitoring the yields of specific $\gamma$ transitions. To scan the HFS of these radioactive isotopes, we have reduced the laser power of the first ionizing step to 5 mW in order to decrease the linewidth of the transitions. This power was sufficient to obtain high enough ion yields, such that in most cases the statistical error on the $\gamma$-line integrals induces a minor source of uncertainty.

#### 1. Results for $^{68}$Cu$^{g,m}$

The simplified schemes of $^{68}$Cu$^g$ ($T_{1/2}=31.1$ s) and $^{68}$Cu$^m$ ($T_{1/2}=3.75$ min) [25] are shown in Fig. 3(a) together with two examples of $\gamma$ spectra: one spectrum corresponds to a laser frequency favoring the high-spin isomer, and another one to a laser frequency favoring the low-spin ground-state production. The measurement time was chosen to be 30 s to enhance the contribution of the $^{68}$Cu$^g$ ions which are produced by a factor of 5 less than the high-spin isomer. The yield of $^{68}$Cu$^m$ ions was monitored by an internal transition (IT) 529 keV $\gamma$-decay line to the $^{68}$Cu$^g$ state (the isomer decays only with a branching ratio of 16% by $\beta$ decay). The yield of $^{68}$Cu$^g$ ions was monitored by the intensity of the 1077.4 keV $\beta$-delayed $\gamma$ transition and was corrected by the intensities of the 1041.3 and 525.9 keV lines [25] to substract feeding from the high-spin isomer. The scans for the $^{68}$Cu$^g$ and $^{68}$Cu$^m$ isomers are shown in Figs 4(a,b). The errors in the ordinate reflect the fluctuations of the laser power and statistical errors. The HFS of the $^{68}$Cu$^g$ atom are well resolved while they are not resolved in the case of the $^{68}$Cu$^m$, implying a smaller nuclear magnetic moment for the isomer. We emphasize again that a scan of the $^{65}$Cu isotope was performed simultaneously at the low-mass beam line of the separator to ensure correct measurements. The width of the Voigt curves in the fitting of the $^{68}$Cu$^g$, $^{68}$Cu$^m$ scans was kept identical to that simultaneously taken at the "low-mass" $^{65}$Cu scans.

It was noticed that in the case of the unresolved overlapping resonance ($^{68}$Cu$^m$ scan) a slightly larger width of the Voigt curves leads to a better fit. This may be due to optical pumping effects that enhance the signal in the center of the scan in the case where the HFS$_g$ are comparable to the linewidth (4 GHz). Here and below we will present the results for the fit of the isomer scans for the same width of the Voigt curves as for the corresponding fits of the ground-state nuclei scans. In the case of the unresolved scans of the isomers we increase the conservative error to 5% due to the possible optical pumping effects.

The deduced atomic ground-state hyperfine splittings, including the scattering error, are 14.7(5) GHz for the $^{68}$Cu$^g$ nuclear ground state and 5.3(3) GHz for the isomeric state. For atomic transitions between electron spin $J=1/2$ states, the HFS are related to the nuclear magnetic moment and the nuclear spin $I$ as follows [20]:

$$\text{HFS} = A\cdot(I+1/2) = \mu B_J\cdot J\cdot\frac{(I+1/2)}{I}, \quad (1)$$

where $A$ is the hyperfine dipole coupling constant, $B_J$ is the hyperfine field, and $J$ is the electron spin. The isotope-independent hyperfine field $B_J$ can be deduced from the known magnetic moment ($\mu=2.38161(19)\mu_N$) and HFS$_g$ of the $I=3/2$ $^{65}$Cu ground state [23], giving $B_J\cdot J =3.9584(3)$ GHz/$\mu_N$. Thus the magnetic moment can be deduced from the measured HFS$_g$ of each nuclear state, provided its nuclear spin is known (or a certain spin is assumed).

The extracted values for the magnetic moments are

$$\mu(^{68}\text{Cu}^g, I=1) = +2.48(2)(7)\mu_N,$$

$$\mu(^{68}\text{Cu}^m, I=6) = +1.24(4)(6)\mu_N,$$

where the quoted errors are the error of the fit and the adopted scattering error, respectively. The sign of the magnetic moments is positive corresponding to the more intense left peak of the scanning curve.

#### 2. The results for $^{70}$Cu$^{g,m_1,m_2}$

A first attempt to measure the HFS of $^{70}$Cu has been reported in Ref. [19]; unfortunately the scan was stopped abruptly due to technical problems with the laser setup. Therefore the obtained values of the magnetic moments have large experimental errors. We have repeated these measurements under better conditions.

Two $\beta$-decaying states in $^{70}$Cu, one feeding low-spin states ($T_{1/2}=5$ s) and one high-spin states ($T_{1/2}=42$ s), have been observed [25]. A 10 s measurement time after each implantation was chosen to enhance the counting from the low-spin isomer. During the monitoring of the intensities of various $\gamma$ transitions as a function of the laser frequency we have observed three different types of behavior giving evidence for the existence of three $\beta$-decaying states. As will be clear from the results and discussion below these nuclei states most likely correspond to $1^+$, $6^-$, and $3^-$ isomers with corresponding half-lives of 6.6(2) s, 44.5(2) s, and 33(2)
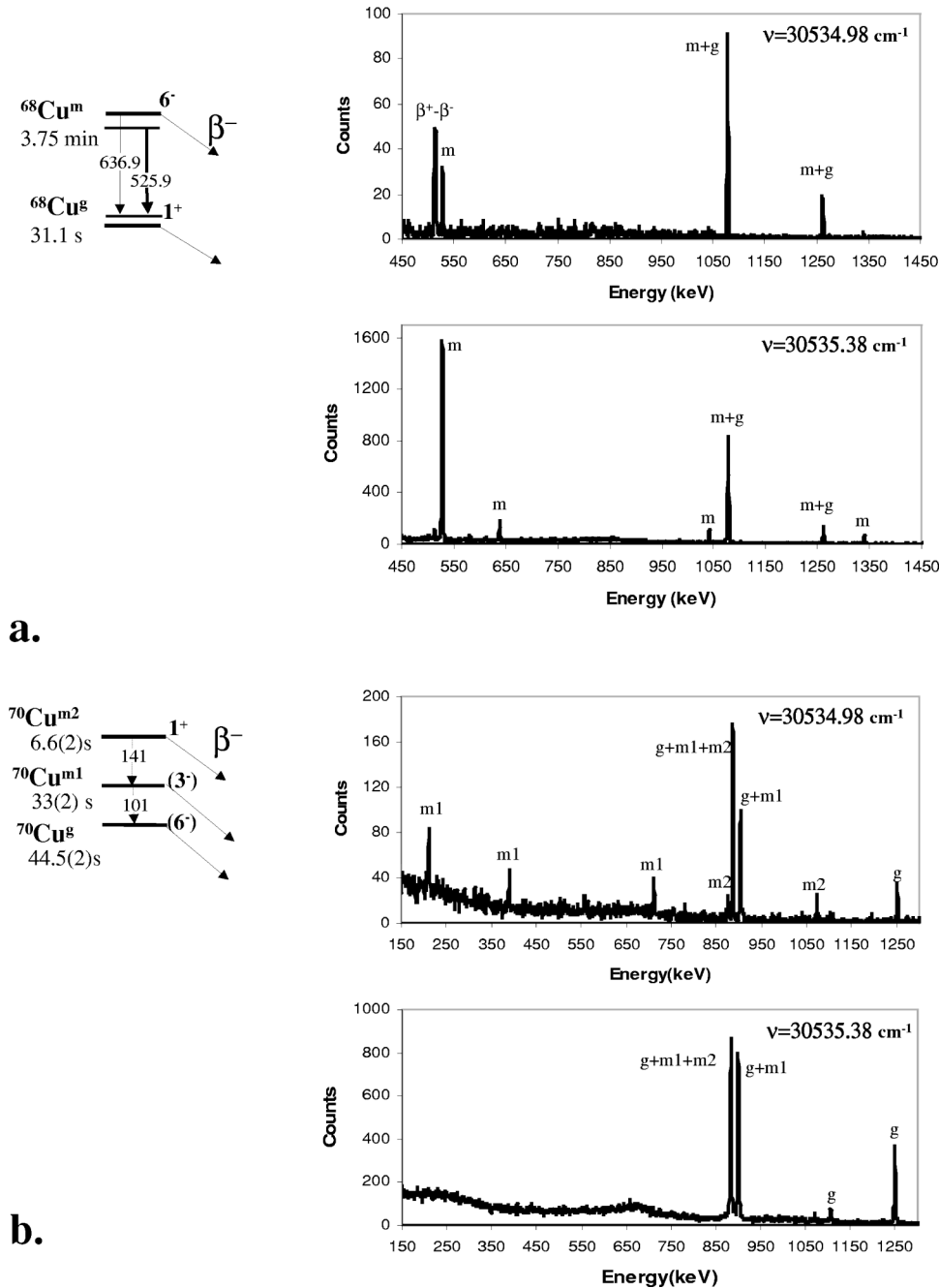
FIG. 3. Simplified decay of $^{68}$Cu and $^{70}$Cu and samples of their $\gamma$ spectra for the two frequencies 30 534.98 cm$^{-1}$ and 30 535.38 cm$^{-1}$ corresponding to preferential ionization of the low- and high-spin states: (a) $^{68}$Cu$^g$ and $^{68}$Cu$^m$; (b) $^{70}$Cu$^g$, $^{70}$Cu$^{m_1}$, and $^{70}$Cu$^{m_2}$. The decay scheme is based on Ref. [12].

s, correspondingly. The relative placement of the isomers is presented in Fig 3(b). Note that two isomers also decay through internal transitions (IT's). The 141 keV IT between $^{70}$Cu$^{m_2}$ and $^{70}$Cu$^{m_1}$ isomers is rather weak (a few percent of the total number of decays). Therefore the feeding between the two isomers causes a small effect on the laser scans. The branching ratio for the 101 keV IT from the $^{70}$Cu$^{m_1}$ isomer is much higher ($\approx 50\%$). However, due to the relatively low production rate for the latter isomer and the short measurement time of 10 s the internal decay does not distort significantly the laser scan results for $^{70}$Cu$^g$. The arguments for the presented placement of the isomers, as well as details on the decay of each individual state, will be addressed in a future publication [12]. The scans corresponding to the three isomers are presented in Figs. 5(a,b,c). The scan in Fig. 5(a)

was obtained by monitoring a strong 1252 keV transition which is fed only in decay of the high-spin $^{70}$Cu$^g$ isomer. The magnetic moment obtained from the scan is

$$\mu(^{70}\text{Cu}^g) = (+)1.50(7)(8)\mu_N.$$

The positive sign of the magnetic moment can be assigned tentatively.

The scan shown in Fig. 5(b) was obtained by monitoring intensities of 101, 209, 387, 553, and 709 keV transitions. All these transitions, except for the 101 keV IT one, originate from a 3246 keV excited level in $^{70}$Zn [12]. The shape of the scan curve in Fig. 5(b) is significantly different indicating the existence of a new $^{70}$Cu$^{m_1}$ isomer, which has a main $\beta$-decay branch ratio to the 3246 keV level. The inverse amplitudes
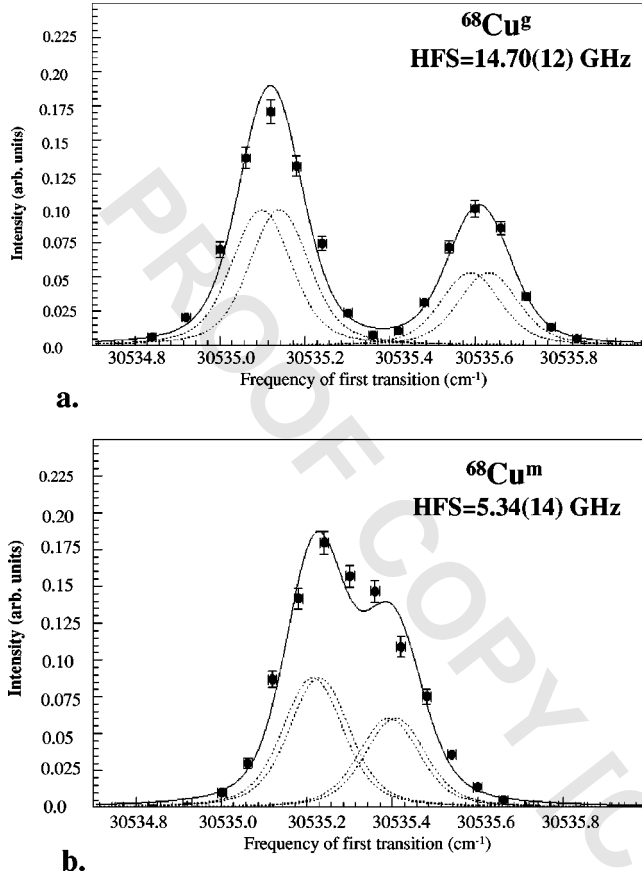
FIG. 4. The results of laser scans for $^{68}$Cu$^g$ (a) and $^{68}$Cu$^m$ (b) isomers. The deduced HFS$_g$ and fit errors are given.

ratio of the scan bumps points to a negative magnetic moment for the isomer. The obtained value of the magnetic moment is

$$\mu(^{70}\text{Cu}^{m_1}) = (-)3.50(7)(11)\mu_N.$$

The nuclear spins $I = 6$ and $I = 3$ were used in Eq. (1) for extraction of the magnetic moment of $^{70}$Cu$^g$ and $^{70}$Cu$^{m_1}$, correspondingly (see discussion).

Finally, the low-spin $^{70}$Cu$^{m_2}$ isomer can be monitored by 141 keV IT and by a 874 keV transition, which is free from any significant feeding from other isomers. The result of these measurements gives

$$\mu(^{70}\text{Cu}^{m_2})(I=1) = +2.07(14)(6)\mu_N.$$

The deduced magnetic moment of $^{70}$Cu$^{m_2}$ has large errors due to poor statistics. Therefore, we performed an alternative measurement, using the large differences in half-lives between $^{70}$Cu$^{m_2}$ and other $\beta$-decaying states. The counting rate in the $4\pi\beta$ detector was monitored as a function of time for about 1.5 to 2 min after the implantation, and for each applied laser frequency. The decay curves were fitted by two exponential decays, one with the half-life of the low-spin isomer [6.6(2)s], and another exponential decay had a half-life as a free parameter and corresponds to an effective long-lived isomer. During the scan the fit result for the latter half-life varied in the range of 35–48 s reflecting different
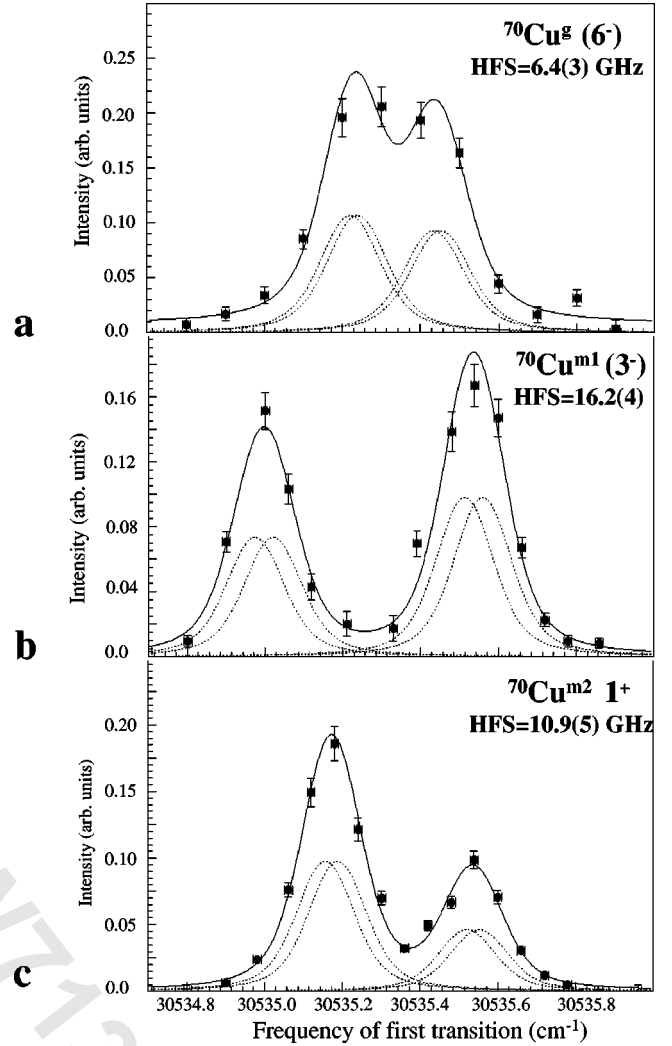


FIG. 5. The results of laser scans for $^{70}$Cu$^g$ (a), $^{70}$Cu$^{m_1}$ (b), and $^{70}$Cu$^{m_2}$ (c) isomers. The laser scan for $^{70}$Cu$^{m_2}$ (1$^+$) was obtained from fitting the decay curves. The deduced HFS and fit error are quoted.

relative productions of two $^{70}$Cu$^{g,m_1}$ long-lived isomers. The isobaric $^{70}$Ga contamination having a long half-life ($T_{1/2} = 21.15$ min) corresponded to a constant background into the fits. As a result of these fits we obtained the $\beta$ intensity of the short-lived component as a function of the laser frequency [Fig 5(c)]. The extracted magnetic moments, $\mu(^{70}\text{Cu}^{m_2}) = +1.84(4)(6)$, are in agreement with the data obtained from monitoring the $\gamma$-line intensities. The $^{70}$Cu$^{m_2}$ magnetic moment obtained from the two measurements is[1]

$$\mu(^{70}\text{Cu}^{m_2}, I=1) = +1.86(4)(6)\mu_N.$$

### III. DISCUSSION

The nuclei around $Z = 28$ and $N = 40$ are expected to be described in terms of single particles coupled to the $^{68}$Ni

---

[1]Only statistical errors from the fits were used for averaging the two measurements.

PROOF COPY [CW7137] 029201PRC

MAGNETIC MOMENTS OF $^{68}$Cu$^{g,m}$ AND $^{70}$Cu$^{g,m_1,m_2}$ . . .

PHYSICAL REVIEW C **65** 0143XX

TABLE II. Comparison of the experimental magnetic moments with calculated values obtained by the additivity theorem using as $\pi p_{3/2}$, $\nu p_{1/2}$, and $\nu g_{9/2}$ single-particle magnetic moments the Schmidt values and the empirical values obtained from the $^{67}$Ni, $^{67}$Cu, $^{69}$Cu, $^{71}$Cu, and $^{67}$Zn measurements (Refs. [9,28,25]). All magnetic moments are in $\mu_N$ units.

| | Schmidt | Empirical (set 1) | Empirical (set 2) | Experimental values |
|---|---|---|---|---|
| Odd proton $\pi p_{3/2}$ | +3.79 | + 2.56 ($\langle ^{71}$Cu,$^{69}$Cu$\rangle$) | + 2.69($\langle ^{69}$Cu,$^{67}$Cu$\rangle$) | |
| Odd neutron $\nu p_{1/2}$ | +0.637 | + 0.6053 ($^{67}$Ni) | + 0.6053 ($^{67}$Ni) | |
| Odd neutron $\nu g_{9/2}$ | −1.91 | − 1.097 ($^{67}$Zn) | − 1.097 ($^{67}$Zn) | |
| $^{68}$Cu$^g$ $1^+$ $\pi p_{3/2}\nu p_{1/2}^{-1}$ | +2.84 | | +1.94 | +2.48(2)(7) |
| $^{70}$Cu$^{m_2}$ $1^+$ $\pi p_{3/2}\nu p_{1/2}^{-1}$ | +2.84 | +1.83 | +1.86(4)(6) | |
| $^{68}$Cu$^m$ $6^-$ $\pi p_{3/2}\nu g_{9/2}$ | +1.88 | | +1.46 | +1.24(4)(6) |
| $^{70}$Cu$^g$ $(6^-)\pi p_{3/2}\nu g_{9/2}$ | +1.88 | +1.59 | | (+)1.50(7)(8) |
| $^{70}$Cu$^{m_1}$ $(3^-)\pi p_{3/2}\nu g_{9/2}$ | −4.59 | −2.92 | | (-)3.50(7)(11) |

core. The protons above the $Z=28$ shell closure will fill the $\pi p_{3/2}$ orbitals. Below $N=40$ the neutrons occupy the $p_{3/2}f_{5/2}$ and $p_{1/2}$ orbitals while above, the $g_{9/2}$ shell is filled. Therefore magnetic moments of $^{68}$Cu$^g$ and $^{70}$Cu$^{m_2}$ should correspond to the $\pi p_{3/2}\nu p_{1/2}^{-1}$ configuration, while those of $^{68}$Cu$^m$ and $^{70}$Cu$^{m_1,g}$ should correspond to the $\pi p_{3/2}\nu g_{9/2}$ configuration. Theoretical calculations show that the application of $^{68}$Ni as a core is quite successful [26]. The negative parity states of $^{69}$Ni are, however, interpreted as $\nu p_{1/2}$ and $\nu f_{5/2}$ holes coupled to a $^{70}$Ni core [7].

It is of interest to investigate how well the measured magnetic moments agree with the extreme single-particle model prediction given by the additivity relation [27]. In Table II the experimental magnetic moments of $^{68,70}$Cu nuclei are compared to calculated values obtained from the additivity relation using the $\pi p_{3/2}$, $\nu p_{1/2}$, and $\nu g_{9/2}$ single-particle magnetic moments from the Schmidt values and the empirical single-particle values obtained from the $^{67}$Ni, $^{67}$Cu, $^{69}$Cu, $^{71}$Cu [9,28], and $^{67}$Zn [29] experimental values. The averaged magnetic moment of the $^{71}$Cu and $^{69}$Cu nuclei was used as the best $\pi p_{3/2}$ single-particle estimate for $^{70}$Cu nuclei while the corresponding averaged value of the $^{69}$Cu and $^{67}$Cu magnetic moments was used for the $^{68}$Cu case. As has been observed in the early 1950's [30] such estimation based on empirical single-particle moments provides quite reliable results over the whole nuclear chart, although even the use of the Schmidt values frequently provides surprisingly good estimations [31]. Indeed, as it is seen in Table II the measured magnetic moments of $^{70,68}$Cu are within 20% agreement with the calculated values. A possible explanation of the somewhat larger disagreement between the empirical estimate and the experimental value in $^{68}$Cu$^g$ can be an admixture of the ground state with excited $1^+$ levels. Such an admixture of the $\pi(f_{7/2}^{-1}p_{3/2}^2\nu f_{5/2}^{-1})_{1^+}$ configuration with the ground state may cause an increase of the magnetic moment. Note that in the $^{67}$Ni isotope we have found that the experimental $g$ factor of the $9/2+$ isomer also deviates strongly from the empirical single-particle values [11].

The spin value of the $^{70}$Cu$^g$ state is subject to a certain controversy. The $\pi p_{3/2}\nu g_{9/2}$ configuration leads to a $3^-$, $4^-$, $5^-$, and $6^-$ multiplet. The modified Nordheim rule [32] predicts that from this multiplet the $3^-$ and $6^-$ states will have

the lowest energy and the result of Paar's calculations [33] suggests that the $6^-$ state is the lowest in energy. The 101 keV IT observed in Ref. [12] can be interpreted as the corresponding $M3$ transition between the excited $3^-$ and the $6^-$ ground states. A $5^-$ assignment of the spin and parity for the ground state would not be compatible with the existence of a third $\beta$-decaying state $(3^-)$ in $^{70}$Cu as then a fast $E2$ decay would take all the decay strength. The spin value of the $^{70}$Cu$^g$ high-spin isomer is intimately connected to the spin assignment for the 3038 keV level of $^{70}$Zn since approximately 58% of $^{70}$Cu$^g$ beta decays proceeds via that level [12]. There is some disagreement in the literature regarding the spin assignment for the 3038 keV level. Although this level has been assigned as $4^-$ in the nuclear data sheets and $I=4$ in the table of isotopes [34,25] the results of $(t,p)$ and $(p,p)$ reaction studies [35,36] suggest a $5^-$ assignment for this level.[2] The recent data from a $\beta$-decay spectroscopy experiment [12] suggest that the spin value of the level is larger than 4. In contrast to that, in recent in-beam, multinucleon transfer studies, the $4^+$ assignment for the level was suggested [38]. This assignment is based on a transition from the level at 3038 keV to the first excited $2^+$ state; such a $\gamma$ ray was not observed in our decay study [12].

Also the strong dependence of the deduced magnetic moment on the assumed spin supports $3^-$ and $6^-$ assignments for the $^{70}$Cu$^{m_1}$ and $^{70}$Cu$^g$ isomers. In Fig. 6 the experimental results are compared with the values calculated for the different spins of the $\pi p_{3/2}\nu g_{9/2}$ multiplet. Two sets of calculations corresponding to Schmidt and empirical single-particle values are given (see also Table II). Clearly the $3^-$ and $6^-$ assignments for $^{70}$Cu$^{m_1}$ and $^{70}$Cu$^g$, respectively, are favored. It is quite interesting to observe in Fig. 6 that the averaging of the calculated magnetic moments based on the Schmidt and the empirical single-particle values provides the better agreement with the experimental results.

Note that Ishii *et al.* [39] come to a similar conclusion regarding the spin assignment when they discuss the members of the $\pi p_{3/2}\nu g_{9/2}$ multiplet suggested from a

---

[2]In the earlier evaluation the $5^-$ state was also assigned for the 3038 keV level [37].
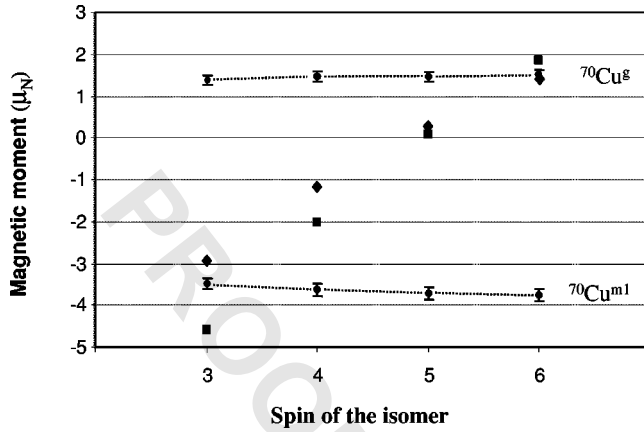
## IV. CONCLUSION

The applicability of in-source spectroscopy to magnetic moment measurements of radioactive nuclei has been demonstrated. The advantage of the method is its high efficiency which allows measurements of magnetic moments of more exotic nuclei by application of $\beta$, $\gamma$, neutron, and $\alpha$ detection. The use of the high-resolution $\gamma$ detectors (or charged particle detectors in the case of $\alpha$ emitters [42]) is more important in the case of a mixture of several isomers, since the HFS of all isomers can be measured during the same laser scan. As an alternative to monitoring the intensities of individual $\gamma$ rays the fitting of decay curves can be used to obtain the same information.

A disadvantage of in-source spectroscopy is the large linewidth due to the strong Doppler broadening which hampers the analysis of the scanned intensity curves. In the case of heavier nuclei the Doppler broadening is reduced and, thus, more accurate measurements are possible.

In this work we have measured the magnetic moments of $^{68}Cu^{g,m}$ and $^{70}Cu^{g,m_1,m_2}$. The results can be explained qualitatively by a simple model with single particles coupled to the $^{68}Ni$ core. The measured magnetic moment of the high-spin isomer in $^{70}Cu$ indicates that $I^\pi = 6^-$ is probably the spin/parity assignment to this state.

The scan obtained by monitoring a certain set of $\gamma$ transitions reveals the existence of a new isomer in $^{70}Cu$. The deduced magnetic moment is consistent with an $I^\pi = 3^-$ assignment for the isomer. In general, the in-source scan measurements combined with $\beta$-delayed $\gamma$ spectroscopy is a useful tool for the search of new isomeric states, as well as for the isomers in spin/parity assignments.



FIG. 6. Calculations of the magnetic moment of the $\pi p_{3/2} \nu g_{9/2}$ single-particle configuration as a function of the isomer spin are compared to the experimental results for $^{70}Cu^{g,m_1}$ isomers. Two sets of calculations corresponding to the Schmidt (squares) and empirical (diamonds) single-particle values are given (Table II). The averaged magnetic moment of $^{71}Cu$ and $^{69}Cu$ was used as the best $\pi p_{3/2}$ empirical single-particle estimate for the $^{70}Cu$ nucleus. The experimental magnetic moments depend weakly on the assumed spin of the isomer according to Eq. (1). The dashed lines serve only to guide the eye.

$^{70}Zn(^3He,t)^{70}Cu$ measurement [40]. The $6^-$ assignment for the $^{70}Cu^g$ isomer also fits into the systematics of the $6^-$ states in the lighter $^{68,66,64}Cu$ isotopes [25]. The magnetic moments of $^{70}Cu^g$, $^{68}Cu^m$ are compared in Table III with those of $^{64}Cu^m$, $^{66}Cu^m$ measured in Ref. [41] by time-differential perturbed angular correlation methods. As it is seen from Table III the magnetic moments of all $6^-$ isomers are reasonably close to the calculated empirical values.

In conclusion, the naive two single particles plus $^{68}Ni$ core description of $^{68,70}Cu$ nuclear states provides good estimations for magnetic moment values although for some isotopes the estimations are about 20% off. It is not possible based on these results to obtain any conclusion regarding the magicity of the $^{68}Ni$ core.

## APPENDIX

Apart from the simplified "equal intensity" fits we have attempted to calculate the intensity ratio for the four atomic transitions which determine the laser scan shape. The transition probabilities have been calculated by taking into account the dependence of the two-photon excitations on the spatial and time power distributions of the exciting laser beams, on the linear polarization of the exciting lasers (causing a nonuniform population of the magnetic sublevels of the hyperfine levels), and on the nuclear spin determining the hyperfine $F$-quantum numbers. In this model the lifetime of the intermediate state, a possible delay between the lasers' pulses, and possible optical pumping and coherence effects during the laser pulse duration have not been taken into account [43]. The relative intensities for the four transitions can then be calculated as a function of the nuclear spin and the laser power. The obtained relative intensities are given in Table IV. All intensities are calculated for the 5 mW laser power of the first step and vary slightly with increasing laser

TABLE III. Comparison of the experimental $6^-$ isomeric magnetic moments in $^{64,66,68,70}Cu$ nuclei to the calculated empirical moments assuming a pure $\pi p_{3/2} \nu g_{9/2}$ configuration. The empirical calculations are based on the $g$ factors for the $3/2^+$ state in $^{63,65,67,69}Cu$ and the $9/2^-$ state in $^{67}Zn$ (Ref. [9,28,29]).

| Nucleus | Excitation energy (keV) | Experimental moments ($\mu$) | Empirical moments ($\mu$) |
|---------|-------------------------|------------------------------|---------------------------|
| $^{64}Cu^m$ | 1594 | +1.06(3) | +1.21 |
| $^{66}Cu^m$ | 1154 | +1.038(3) | +1.36 |
| $^{68}Cu^m$ | 721.6 | +1.24(4)(6) | +1.46 |
| $^{70}Cu^g$ | (0) | (+)1.50(7)(8) | +1.59 |

PROOF COPY [CW7137] 029201PRC

MAGNETIC MOMENTS OF $^{68}Cu^{g,m}$ AND $^{70}Cu^{g,m_1,m_2}$ . . .

PHYSICAL REVIEW C **65** 0143XX

TABLE IV. Relative intensities of the four transitions involved in the resonant excitation of the Cu atoms, with respect to the intensity in line #1, as a function of the nuclear spin and the laser power, calculated using the model described in Ref. [43]. All intensity ratios are calculated for 5 mW laser power of the first ionizing step.

| Spin | $I_1$ | $I_2$ | $I_3$ | $I_4$ |
|------|-------|-------|-------|-------|
| 3/2 | 1 | 0.255 | 1.185 | 1.270 |
| 1 | 1 | 0.193 | 1.848 | 1.534 |
| 2 | 1 | 0.366 | 1.200 | 1.214 |
| 3 | 1 | 0.425 | 0.974 | 1.117 |
| 4 | 1 | 0.452 | 0.859 | 1.074 |
| 5 | 1 | 0.466 | 0.786 | 1.051 |
| 6 | 1 | 0.475 | 0.741 | 1.038 |

power value. The calculated intensity ratios allow to reduce the number of free fit parameters to five: the position of peak 1, the intensity of peak 1, the linewidth, a constant background, and the atomic ground-state HFS. An example of such a fit for the $^{65}$Cu laser scan for the 1.5 mW laser power of the first laser step is shown in Fig. 7(a). Using these additional conditions on the relative peak intensities, we obtained the fit results for the $^{65}$Cu laser scans for the various laser power values. The adopted values for $^{65}$Cu HFS and the central frequency, as deduced from these "relative intensity" fits, are 12.30(35) GHz and 30535.33(2) cm$^{-1}$, respectively. These results are in good agreement with the "equal intensity" fit result and the literature value (Table I). The "equal intensity" fit seems to give a better agreement for the deduced HFS, whereas the "relative intensity" fit gives a better agreement for the central frequency. The fits with "relative amplitudes" of the stable $^{65}$Cu laser scans are quite satisfactory considering the reduced number of fitting parameters. The corresponding fits of the $^{68,70}$Cu$^m$ scan curves also yield good agreement with the "equal intensity" results [Fig. 7(c)]. However we have not managed to obtain a good fit with calculated relative intensities for odd-odd $^{68,70}$Cu$^g$ isotopes. An example of such a fit for $^{68}$Cu$^g$ is presented in Fig. 7(b). It is very surprising that by using the relative amplitudes corresponding to an $I = 2$ nuclear spin (Table IV) one can obtain a good fit. However, from the spectroscopy data one can confidently claim that the ground state of $^{68}$Cu corresponds to the nuclear spin $I = 1$. It is most likely that not all physical phenomena are appreciated in the model. Further theoretical efforts are needed to provide better understanding of the scanning curves obtained with the in-source spectroscopy method. It is clear however from the examples pre-
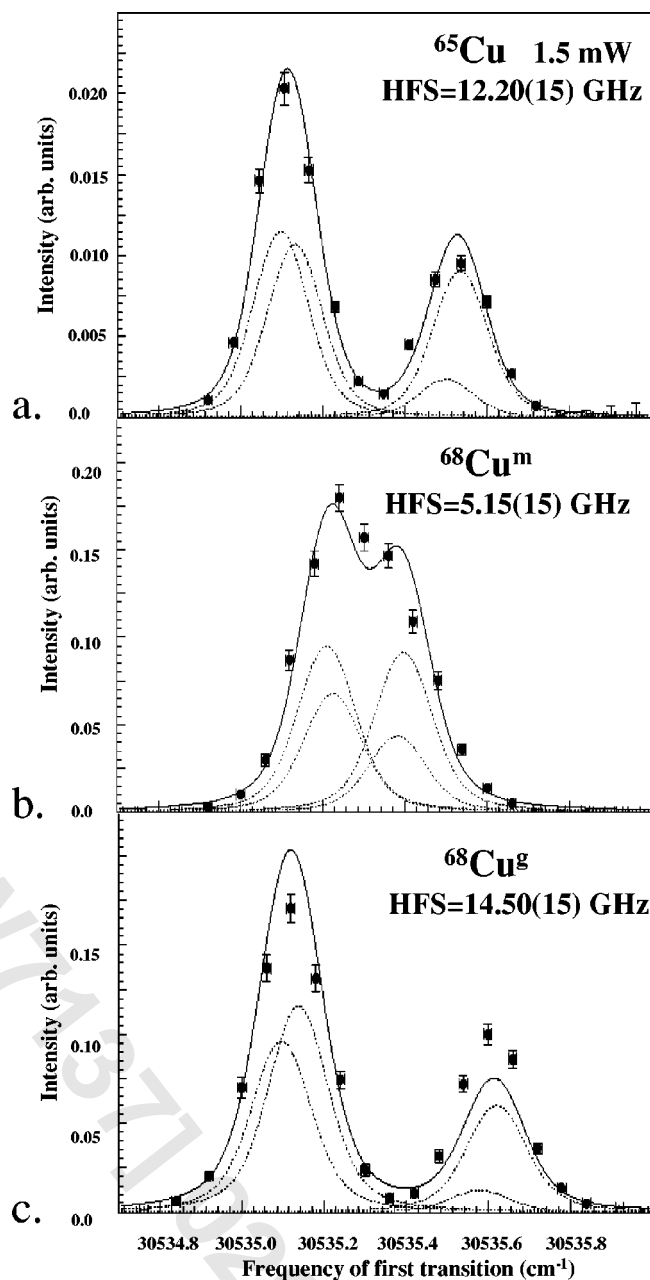


FIG. 7. The "relative intensity" fits with amplitude ratios from Table IV performed for (a) a laser scan of $^{65}$Cu at 1.5 mW the first laser step power, (b) $^{68}$Cu$^m$, and (c) $^{68}$Cu$^m$ scans. The deduced HFS $_g$ and fit errors are given and can be compared with the corresponding results of the "equal intensity" fits [Figs. 2 and 4(a,b)].

sented in Figs. 2, 4,and 7 that whatever fitting method is used in the analysis of the laser scans, the extracted atomic HFS and, hence, the nuclear magnetic moments are close within the quoted errors.

[1] R. Broda *et al.*, Phys. Rev. Lett. **74**, 868 (1995).
[2] Ch. Engelman *et al.* Z. Phys. A **352**, 351 (1995).
[3] F. Ameil *et al.*, Eur. Phys. J. A **1**, 275 (1998).
[4] R. Grywacz *et al.*, Phys. Rev. Lett. **81**, 766 (1998).

[5] S. Franchoo *et al.*, Phys. Rev. Lett. **81**, 3100 (1998).
[6] L. Weissman *et al.*, Phys. Rev. C **59**, 2004 (1999).
[7] W.F. Mueller *et al.*, Phys. Rev. Lett. **83**, 3613 (1999).
[8] W.F. Mueller *et al.*, Phys. Rev. C **61**, 054 308 (2000).

[9] J. Rikovska *et al.*, Phys. Rev. Lett. **85**, 1392 (2000).

[10] G. Neyens *et al.*, Nucl. Phys. A ■, ■ (2001); Proceedings of the Fifth *Conference on Radioactive Nuclear Beams* (to be published ■■■)

[11] G. Georgiev *et al.*, Phys. Rev. Lett. (to be published ■■■).

[12] J. Van Roosbroeck *et al.* (to be published ■,■,■; K. Krouglov *et al.* (to be published ■■■).

[13] V.I. Mishin, V.N. Fedoseyev, H.-J. Kluge, V.S. Letokov, H.L. Ravn, F. Scheerer, Y. Shirakabe, S. Sundell, O. Tengblad, and ISOLDE Collaboration, Nucl. Instrum. Methods Phys. Res. B **73**, 550 (1993).

[14] Y. Kudryavtsev *et al.*, Nucl. Instrum. Methods Phys. Res. B **114**, 350 (1996).

[15] G.D. Alkhazov *et al.*, Nucl. Instrum. Methods Phys. Res. B **69**, 517 (1992).

[16] A.E. Barzakh, I.Ya. Chubukov, D.V. Fedorov, V.N. Panteleev, M.D. Seliverstov, and Yu.M. Volkov, Phys. Rev. C **61**, 034 304 (2000).

[17] A.E. Barzakh, D.V. Fedorov, T.T. Fedorov, V.S. Ivanov, F.V. Moroz, V.N. Panteleev, M.D. Seliverstov and Yu. M. Volkov, Russian Academy Petersburg Nuclear Physics Institute, preprint 2413.

[18] V. Sebastian *et al.*, in *ENAM 98, Exotic Nuclei and Atomic Masses*, edited by Brodley M. Sherill, David M. Morissey, and Cary N. Davids, AIP Conf. Proc. No.**455** (AIP, Woodbury, NY, 1998), p. 126.

[19] U. Köster *et al.*, Nucl. Instrum. Methods Phys. Res. B **160**, 528 (2000).

[20] E.W. Otten, *Treatise on Heavy-Ion Science* (Plenum Press, New York, 1988), Vol. 8, p. 517.

[21] U. Köster *et al.* (unpublished).

[22] V.N. Fedoseyev, G. Huber, U. Köster, J. Lettry, V.I. Mishin, H. Ravn, and V. Sebastian, Hyperfine Interact. **127**, 409 (2000).

[23] H. Figger, D. Schmitt, and S. Penselin, Colloq. Int. C. N. R. S. **164**, 355 (1967).

[24] H. Bergström, W.X. Peng, and A. Persson, Z. Phys. D: At., Mol. Clusters **13**, 203 (1989).

[25] R.B. Firestone, *Tables of Isotopes*, 8th ed. (Wiley, New York, 1996).

[26] A.M. Oros-Peusquens, and P.F. Mantica, Nucl. Phys. **A669**, 81 (2000).

[27] R.J. Blin-Stoyle, Rev. Mod. Phys. **28**, 75 (1956).

[28] J. Rikovska *et al.* (unpublished).

[29] P. Raghavan, At. Data Nucl. Data Tables **42**, 189 (1989).

[30] H.M. Schwartz, Phys. Rev. **89**, 1293 (1953).

[31] E. Feenberg, Phys. Rev. **76**, 1275 (1949).

[32] M.H. Brennan and A.M. Bernstein, Phys. Rev. **120**, 927 (1960).

[33] V. Paar, Nucl. Phys. **A331**, 16 (1979).

[34] M.R. Bhat, Nucl. Data Sheets **68**, 117 (1993).

[35] F.R. Hudson, Nucl. Phys. **A189**, 264 (1972).

[36] J. Jabbour, Nucl. Phys. **A490**, 245 (1988).

[37] F. Kearn, and J.N. Mo, Nucl. Data Sheets **25**, 1 (1978).

[38] A.N. Wilson, C.W. Beausang, N. Amzal, D.E. Appelbe, S. Asztalosl, P.A. Butler, R.M. Clark, P. Fallon, and A.O. Macchiavelli, Eur. Phys. J. A **9**, 183 (2000).

[39] T. Ishii, M. Asai, I. Hossain, P. Kleinheinz, M. Ogawa, A. Makishima, S. Ichikawa, M. Itoh, M. Ishii, and J. Blomqvist, Phys. Rev. Lett. **81**, 4100 (1998).

[40] J.D. Sherman, E.R. Flynn, O. Hansen, N. Stein, and J.W. Sunier, Phys. Lett. **67B**, 275 (1977).

[41] J. Bleck, R. Butt, K.H. Lindenberger, W. Ribbe, and W. Zeitz, Nucl. Phys. **A197**, 620 (1972).

[42] A. Andreyev *et al.* (unpublished).

[43] S. Gheysen, Diploma thesis ■,■■ K.U. Leuven (unpublished); S. Gheysen *et al.* (unpublished).